Appl Phys B (2011) 104:747–754
DOI 10.1007/s00340-011-4596-y

Applied Physics B
Lasers and Optics

Highly efficient and broadband Si homojunction structured near-infrared light emitting diodes based on the phonon-assisted optical near-field process

T. Kawazoe · M.A. Mueed · M. Ohtsu

Received: 27 April 2011 / Published online: 16 June 2011
© The Author(s) 2011. This article is published with open access at Springerlink.com

Abstract We fabricated a highly efficient, broadband light emitting diode driven by an optical near field generated at the inhomogeneous domain boundary of a dopant in a homojunction bulk Si crystal and evaluated its performance. To fabricate this device, a forward current was made to flow through a Si p–n junction to anneal it. During this process, the device was irradiated with near-infrared light, producing stimulated-emission light using a two-step phonon-assisted process triggered by the optical near field, and the annealing rate was controlled in a self-organized manner. The device emitted light in a wide photon energy region of 0.73–1.24 eV (wavelength 1.00–1.70 µm). The total power of the emitted light with 11 W of electrical input power was as high as 1.1 W. The external power conversion efficiency of the emitted light was 1.3%, the differential external power conversion efficiency was 5.0%, the external quantum efficiency was 15%, and the differential external quantum efficiency was 40%. The dependency of the emitted light power density on the injected current density clearly showed a characteristic reflecting the two-step phonon-assisted transition process.

T. Kawazoe (✉) · M.A. Mueed · M. Ohtsu
Department of Electrical Engineering and Information Systems, Graduate School of Engineering, The University of Tokyo, 2-11-16 Yayoi, Bunkyo-ku, Tokyo 113-8656, Japan
e-mail: kawazoe@ee.t.u-tokyo.ac.jp
Fax: +81-3-58411140

T. Kawazoe · M. Ohtsu
Nanophotonic Research Center, Graduate School of Engineering, The University of Tokyo, 2-11-16 Yayoi, Bunkyo-ku, Tokyo 113-8656, Japan

1 Introduction

The emission wavelength of semiconductor light emitting diodes (LEDs) is determined by the bandgap energy, E_g, of the materials used. For example, to realize near-infrared LEDs that emit in the wavelength range 1.00–1.70 µm (photon energies 0.73–1.24 eV), which contains the optical fiber communication band, InGaAsP, a direct transition type semiconductor, is used [1, 2]. To achieve high-efficiency light emission, it is necessary to employ a complex double-heterojunction structure that uses an InGaAsP active layer and an InP carrier confinement layer epitaxially grown on an InP substrate. The shortcomings of this approach are that InP is highly toxic [3], and In is a rare material. Silicon (Si), on the other hand, is a semiconductor having low toxicity and no concerns about depletion of resources; however, its emission efficiency is low because it is an indirect transition type semiconductor. Therefore, until now it has been considered unsuitable as a material for use in LEDs. However, because of the growing concern over environmental issues, LEDs using Si have recently been investigated. For example, in the visible region, porous Si [4], Si/SiO_2 superlattice structures [5, 6], and Si nanoprecipitates in SiO_2 [7] have been used, and in the infrared region, erbium-doped Si [8] and Si–Ge [9] have been used. However, their emission efficiencies are still low. For example, the external quantum efficiency and power conversion efficiency of an LED using a sub-bandgap transition in Si [10] are 0.5% and 0.8%, respectively.

In this study, using bulk crystal Si having a homojunction that is extremely simple compared with the structures described above, we varied the spatial distribution of the dopant density in the Si by a novel annealing process using a phonon-assisted process induced by an optical near field [11] to fabricate a highly efficient, broadband LED. The

light emission wavelength covered the optical fiber communications band.

2 Principles of light emission

The phonon-assisted process [11] originates from the property that an optical near field couples with a phonon; when it is used, however, even if light having a photon energy $h\nu$ smaller than the bandgap energy E_g of the semiconductor is incident, an electron–hole pair is created. The reason for this is that it is possible for electrons in the valence band to be excited to the conduction band via an electric dipole forbidden transition to the phonon level, because the optical near field is a quasiparticle representing a virtual exciton–phonon–polariton state in which an exciton polariton and a phonon are coupled in the nano-regime. This excitation is a two-step transition that has already been applied to photochemical vapor deposition [11], photodetectors [12], photolithography [13], subnanometer polishing of glass surfaces [14], frequency up-conversion [15], and so on. This two-step transition is explained as follows (Fig. 1(a)) [11, 16].

(1) First step: Transition from the ground state $|E_g; el\rangle \otimes |E_{ex_{thermal}}; phonon\rangle$, which is the initial state, to an intermediate state $|E_g; el\rangle \otimes |E_{ex}; phonon\rangle$. Here, the ket vector $|E_g; el\rangle$ represents the electronic ground state, and $|E_{ex_{thermal}}; phonon\rangle$ and $|E_{ex}; phonon\rangle$ respectively represent the phonon excitation state that is determined by the crystal lattice temperature, and the phonon excitation state that is determined by the photon energy of the optical near field. The symbol $\otimes$ represents the direct product of the ket vectors representing the two states. Because it is an electric dipole forbidden transition, an optical near field is essential in this excitation.

(2) Second step: Excitation from the intermediate state $|E_g; el\rangle \otimes |E_{ex}; phonon\rangle$ to the final state $|E_{ex}; el\rangle \otimes |E_{ex'}; phonon\rangle$. Here, $|E_{ex}; el\rangle$ represents the electron excitation state, and $|E_{ex'}; phonon\rangle$ represents the phonon excitation state. Because this is an electric dipole allowed transition, the excitation occurs via not only an optical near field but also via propagating light. After this excitation, the phonon excitation state relaxes to a thermal equilibrium state with an occupation probability determined by the lattice temperature and ends with excitation to the electron excitation state $|E_{ex}; el\rangle \otimes |E_{ex_{thermal}}; phonon\rangle$.

It should be noted that there is an inverse process to this process, namely, the two-step spontaneous emission process shown below (Fig. 1(b)) [12]:

(1′) First step: Transition from the initial state $|E_{ex}; el\rangle \otimes |E_{ex_{thermal}}; phonon\rangle$ of the electron in the conduction band to the intermediate state $|E_g; el\rangle \otimes |E_{ex}; phonon\rangle$, which generates spontaneously emitted light. Because this is an electric dipole allowed transition, propagating light and an optical near field can both be generated; however, the process of generating propagating light is limited to the transition to $|E_{ex_{thermal}}; phonon\rangle$ close to $|E_g; el\rangle$. The reason is that the occupation probability of $|E_{ex}; phonon\rangle$ is low in levels other than those close to $|E_g; el\rangle$ which has an energy on the order of kT (where k is Boltzmann's constant, and T is the crystal lattice temperature). In other words, this is because the phonon excitation state $|E_{ex}; phonon\rangle$ is in the thermal equilibrium state since the propagating light does not generate a phonon. On the other hand, the probability of emitting an optical near field does not depend on the occupation probability of the phonon in the thermal equilibrium state, because the optical near field generates a phonon.

(2′) Second step: Transition from the intermediate state $|E_g; el\rangle \otimes |E_{ex}; phonon\rangle$ to the ground state $|E_g; el\rangle \otimes |E_{ex'}; phonon\rangle$. Because this is an electric dipole forbidden transition, only an optical near field is generated. After this transition, the phonon excitation state relaxes to the thermal equilibrium state determined by the crystal lattice temperature and ends with a transition to the electronic ground state $|E_g; el\rangle \otimes |E_{ex_{thermal}}; phonon\rangle$.

Part of the optical near field spontaneously emitted by the above two-step process is converted to observable propagating light, which is observed in the optical far field [12]. Therefore, electrons are excited by current injection, and an LED can be realized utilizing processes (1′) and (2′) above. The emission wavelength of this device is not the bandgap energy E_g, but depends on the photon energy of the optical near field in the vicinity of the p–n junction.

It is well known that a phonon is needed for an indirect transition type semiconductor to spontaneously emit propagating light. This is because, for spontaneous emission, the wavenumber must be conserved (this is known as the wavenumber conservation law). An optical near field, however, has multiple modes that satisfy the wavenumber conservation law because the photons are strongly coupled with multi-mode phonons [11, 16], and the probability of spontaneous emission due to the optical near field is extremely high.

In addition, this phonon-assisted process can also involve a two-step stimulated-emission process explained in the following (Fig. 1(c)).

(1″) First step: When an electron in the conduction band is irradiated with an optical near field, the electron transitions from the initial state $|E_{ex}; el\rangle \otimes |E_{ex_{thermal}}; phonon\rangle$ to the intermediate state $|E_g; el\rangle \otimes |E_{ex}; phonon\rangle$, and light is emitted via stimulated emission.

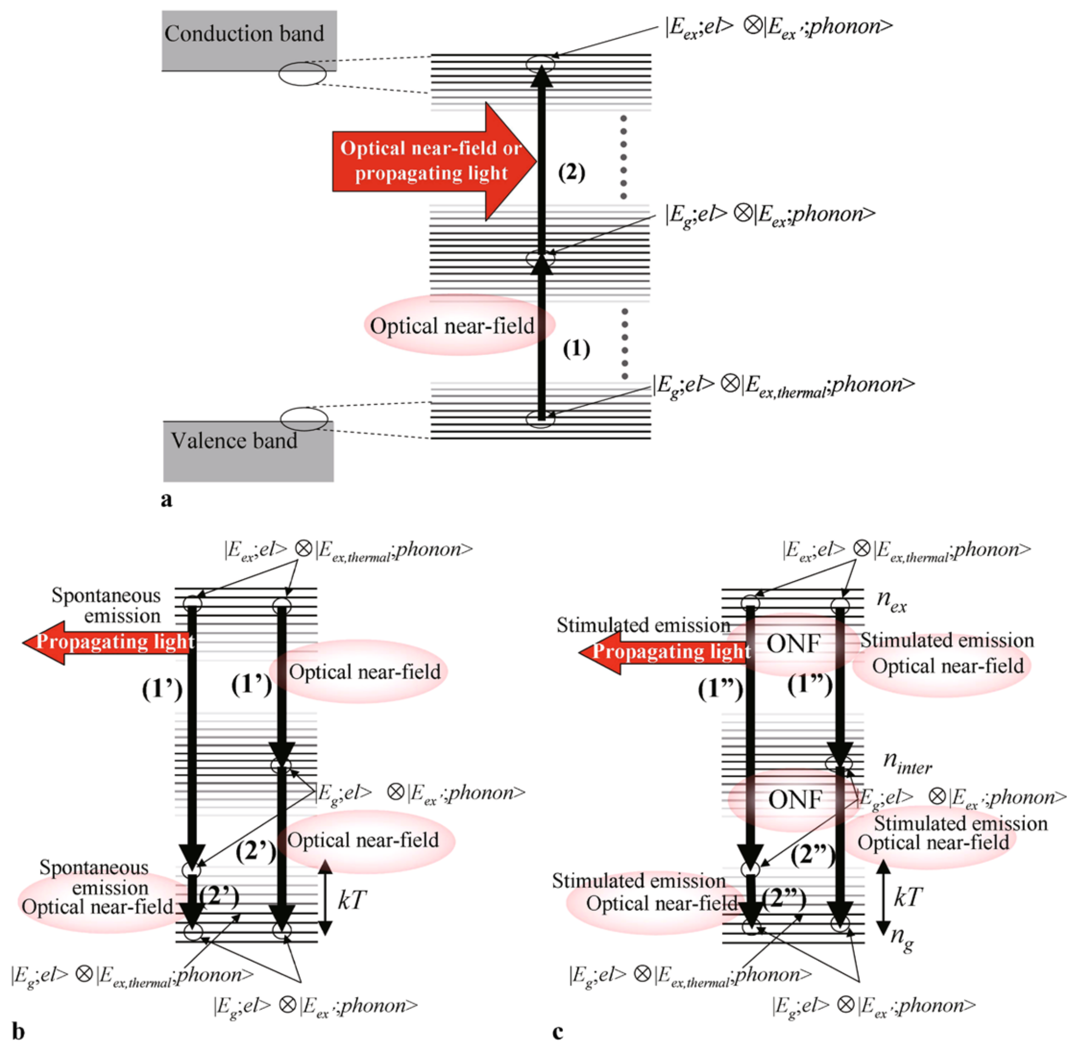

Fig. 1 Three kinds of two-step phonon-assisted processes. (**a**) Excitation of an electron: (1) and (2) represent the first and second steps of the excitation, respectively. (**b**) Spontaneous emission: (1′) and (2′) represent the first and second steps of the transition, respectively. (**c**) Stimulated emission: (1″) and (2″) represent the first and second steps of the transition, respectively. ONF: optical near-field

Similar to the first step (1′) of the spontaneous emission described above, the transition processes that generate propagating light are extremely limited. Here, when the electron number densities of occupation in the initial state $|E_{ex}; el\rangle \otimes |E_{ex_{thermal}}; phonon\rangle$ and the intermediate state $|E_g; el\rangle \otimes |E_{ex}; phonon\rangle$, n_{ex} and n_{inter}, satisfy the Bernard–Duraffourg inversion condition ($n_{ex} > n_{inter}$) [17], the number of photons created by stimulated emission exceeds the number of photons annihilated by absorption.

(2″) Second step: Transition from the intermediate state $|E_g; el\rangle \otimes |E_{ex}; phonon\rangle$ to the final state $|E_g; el\rangle \otimes |E_{ex'}; phonon\rangle$, which emits light via stimulated emission. Because this is an electric dipole forbidden transition, only an optical near field is generated. After this transition, the phonon excitation state relaxes to a thermal equilibrium state determined by the crystal lattice temperature, and ends with a transition to the electronic ground state $|E_g; el\rangle \otimes |E_{ex_{thermal}}; phonon\rangle$.

3 Device fabrication

To realize the device proposed in this paper, we used the two-step phonon-assisted process involving optical near fields two times. The first was for operating the device to obtain spontaneously emitted light, and the experimental results of this are reported in the next section. The second was for fabricating the device, in other words, for self-organized control of the spatial distribution of the dopant density suitable for high-efficiency spontaneous emission. The second usage method is described in this section.

To fabricate the device, As-doped n-type Si crystal wafer, with an electrical resistivity of 10 Ω cm and a thickness of 625 µm was used. The Si crystal wafer was then doped with B using ion implantation to form a p-layer. The B implantation energy was 700 keV, and the ion dose density was 5×10^{13} cm^{-2}. After forming a p–n junction in this way, an indium tin oxide (ITO) layer with a thickness of 150 nm was deposited on the p-layer side, and an Al layer with a thickness of 80 nm was deposited on the n-layer side, both by RF sputtering, and these were used as positive and negative electrodes. Then, the Si crystal wafer with the electrodes attached was diced into a single device. The surface area was about 10 mm^2.

Finally, a forward bias voltage of 16 V was applied (current density, 4.2 A/cm^2) to generate Joule heating for performing annealing, diffusing the B and varying the spatial distribution of its concentration. During this process, laser light (optical power density, 10 W/cm^2) with a photon energy ($h\nu_{anneal} = 0.95$ eV, wavelength 1.30 µm) smaller than the bandgap energy of Si ($E_g = 1.12$ eV) [18] was radiated from the ITO electrode side. This induced a phonon-assisted process, modifying the B diffusion by annealing, and forming characteristic minute inhomogeneous domain boundaries in a self-organized manner. This was due to the following three reasons:

(1) Because the forward bias voltage (16 V) is much higher than E_g (= 1.12 eV), the difference ($E_{Fc} - E_{Fv}$) between the quasi-Fermi energy of the conduction band, E_{Fc}, and the quasi-Fermi energy of the valence band, E_{Fv}, is higher than E_g, thus satisfying the Bernard–Duraffourg inversion condition ($n_{ex} > n_{inter}$). Also, when light with a photon energy $h\nu_{anneal}$ below E_g is radiated, this light propagates in the substrate without being absorbed in the Si and generates an optical near field at the domain boundaries of the inhomogeneous distribution of B [19]. This optical near field excites coherent phonons close to the p–n junction, forming an optical-near-field–phonon coupled state, that is to say, a virtual exciton–phonon polariton. Because the energy of this quasiparticle is equal to the sum of the photon energy and the energy of the induced phonon, even though $h\nu_{anneal} < E_g$, this energy is large enough to cause stimulated emission. Therefore, the electron transitions from the excitation state to the phonon level via an electric dipole forbidden transition due to the incident light with energy $h\nu_{anneal}$ ($< E_g$), and a photon is generated during this transition by stimulated emission.

(2) Part of the Joule heating energy due to the forward bias is spent in the stimulated emission of photons, and therefore, the annealing rate is decreased. That is, at sites where the phonon-assisted stimulated emission in (1) above is easily generated, the shape and dimensions of the B inhomogeneous domain boundaries become more difficult to change. If it is assumed that the shape of the domain boundary is a sphere of radius r, and that r is smaller than the thickness of the active layer, the probability of generating stimulated emission in one domain boundary is proportional to the product of the number of photons incident on the domain boundary, the transition probability, and the volume of the spatial distribution of the optical near field. According to [11], these are proportional to r^2, r^{-2}, and r^3, respectively. Therefore, the probability of stimulated emission (that is, the annealing inhibition rate) is proportional to their product, r^3. On the other hand, because the generated Joule heating is proportional to the current passing through that domain, the annealing rate is proportional to r^2. Therefore, the temporal rate of change of the domain boundary size r (dr/dt) is given by $dr/dt = ar^2 - br^3$ (a and b are constants determined by the forward bias current and optical intensity, respectively), and in the stationary state ($dr/dt = 0$), it becomes $r = a/b$.

(3) Process (2) above occurs in all domain boundaries in the device, not just at one domain boundary. In practice, the sizes and shapes of the domain boundaries are inhomogeneous, even after reaching the stationary state, for various reasons, such as the variety of shapes of the domain boundaries, the presence of a large number of domain boundaries, inhomogeneous current density, and so on. Because the probabilities of stimulated emission and spontaneous emission are proportional to each other [20], phonon-assisted spontaneous emission also tends to occur in regions where the phonon-assisted spontaneous stimulated emission process tends to occur. Therefore, as process (2) proceeds, the generated stimulated emission light irradiates the entire device, and therefore, process (2) does not remain in the light-irradiation region but spreads in a self-organized manner to the entire device. It is expected that the shapes and distribution of the domain boundaries formed in this way will be optimal for efficiently inducing the phonon-assisted process during device operation.

Figure 2(a) is a photograph showing the device during annealing. A W probe was contacted to the positive electrode, a 20 µm-thick Al foil was attached to the negative electrode, and electric power was supplied. The electric power applied to the device was 11 W. Figure 2(b) is a thermography image of the device surface temperature 1 minute after applying the bias current. The surface temperature of the device was 110–220°C. The temporal variation of the surface temperature is shown in Fig. 2(c). After a sudden increase to 154°C by heating due to the bias current, the temperature dropped and reached a stable value (140°C) after about 6 minutes. This temperature variation is consistent with the above discussion related to annealing under light irradiation. Specifically, although the power applied to the device generates Joule heating, raising the temperature, once the optical near field is

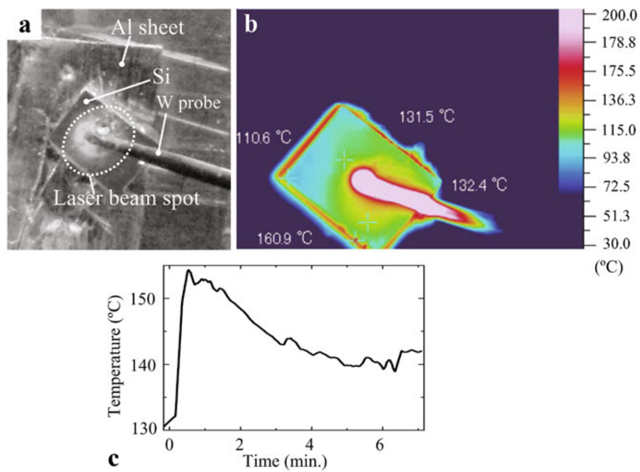

Fig. 2 Temperature variation due to annealing. (**a**) Photograph of device during annealing. (**b**) Surface temperature distribution of device 1 minute after starting annealing. (**c**) Temporal change in temperature at center of device during annealing

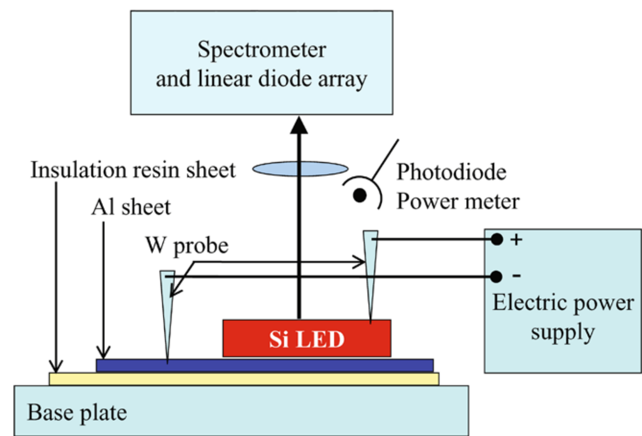

Fig. 3 Experimental setup for evaluating device characteristics

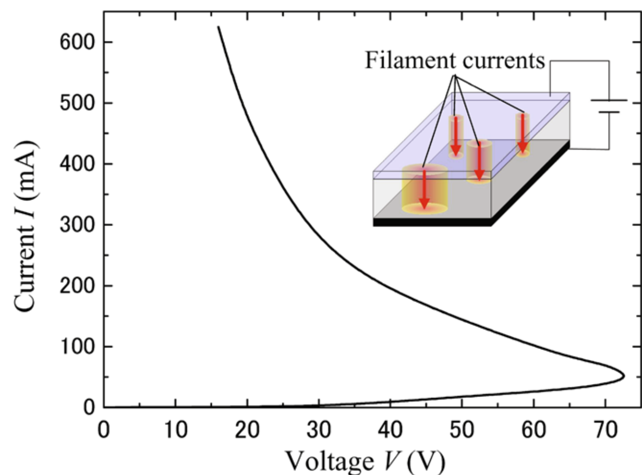

Fig. 4 Relationship between current I and forward bias voltage V applied to device. *Inset* schematically shows filament currents predicted from the experimental results

generated in the domain boundary where the B concentration distribution is inhomogeneous, commencing stimulated emission, part of the Joule heating is dissipated in the form of light, and the temperature drops, soon reaching the stationary state. The forward bias was applied for 30 minutes while irradiating the device with light, which completes the fabrication of the device.

4 Device operation

The experimental setup used for evaluating the characteristics of the fabricated device is shown in Fig. 3. We used a spectrometer and an InGaAs linear photodiode array (Spectra-Physics, Inc., OMA-V1024) to observe the emitted light spectrum. We used an InGaAs photodiode (Hamamatsu Photonics K.K., G8370-83) to observe emitted light in the energy region of 0.73 eV (wavelength 1.70 µm) and above. We used a wideband optical power meter (Spectra-Physics, Inc., 407A) to measure the emitted light intensity in the energy region 0.11–4.96 eV (wavelength 0.25–11.0 µm).

First, Fig. 4 shows the relationship between the injection current to the device, I, and the forward bias voltage, V. In this graph, $I > 50$ mA indicates a negative resistance, and the break over voltage was 73 V [21]. This was due to the spatially inhomogeneous current density [21] and the generation of filament currents, as shown in the inset of Fig. 4. In other words, the B distribution has a domain boundary, and the current is concentrated in that region. A center of localization where the electrical charge is easily bound is formed in this current concentration region, and an optical near field is easily generated there. That is, the negative resistance is the principle of the device fabrication described in the previous section. The reason why the break over voltage is higher than the built-in potential of the Si p–n junction is thought to be because of the high total resistance due to the thick Si crystal wafer, and the large contact resistance between the electrodes and the Si crystal wafer. In addition, although the device surface temperature during annealing (Fig. 2(b)) is too low for diffusing the B, it is thought that localized heating occurs due to the filament currents mentioned above, which makes the temperature inside the device sufficiently high. From secondary ion-microprobe mass spectrometry (SIMS), we confirmed that the B penetration depth was increased to at least 300 nm by the annealing.

Second, Figs. 5(a) and (b) show photographs of the external appearance of the non-biased and forward-biased (current density 4.2 A/cm^2) device taken with an infrared CCD camera (photoreceptor band 0.73–1.38 eV (wavelength 0.90–1.70 µm)) at room temperature and under fluorescent light illumination. Figure 5(b) reveals strong emit-

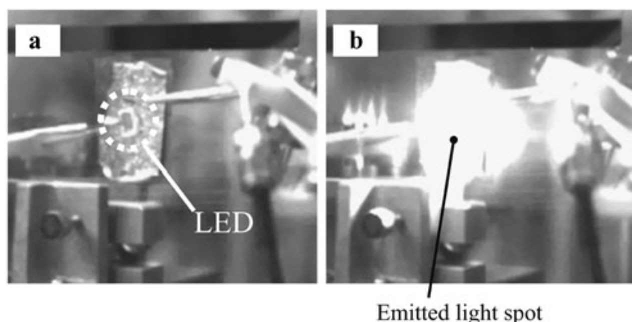

Fig. 5 Photograph of device emitting light at room temperature, captured with an infrared camera under fluorescent light illumination: (**a**) current density $I_d = 0$; (**b**) current density $I_d = 4.2$ A/cm^2

ted light. The injection current at this time was 11 W, and the emitted power reached as high as 1.1 W.

It is well known that commercially available Si photodiodes made by conventional methods emit very small amounts of light. For comparison, therefore, Fig. 6(a) shows the extremely weak emission spectrum when a current density of 0.2 A/cm^2 was made to flow in a commercially available Si photodiode (Hamamatsu Photonics K.K., S3590). The device was destroyed with a current density higher than this. In this graph, like the results in [10], the emission spectrum was distributed on the high-energy side of E_g ($= 1.12$ eV). This was due to phonon scattering in the indirect band structure of the Si.

In contrast, the shape of the emission spectrum of our device differed from that in Fig. 6(a). Figures 6(b)–(d) are the emission spectra of devices fabricated by annealing for 1 min, 7 min, and 30 min, respectively. The bias current density was 1.5 ± 0.5 A/cm^2. Unlike Fig. 6(a), the emission spectrum extended to energies lower than E_g. The decrease in the emission spectral intensity in the energy region below 0.8 eV was due to the sensitivity limit of the photodetector; in reality, the emission spectrum is thought to extend to even lower energies. The device fabricated by annealing for 1 min had an intense emission peak close to E_g, which extended as far as 0.75 eV (wavelength 1.65 µm), as shown in Fig. 6(b). A new emission peak appeared close to 0.83 eV (wavelength 1.49 µm) in the emission spectrum of the device fabricated by annealing for 7 min (Fig. 6(c)). The reason for the particularly small spectral intensity at energies lower than this peak was because of the sensitivity limit of the photodetector. There was no intense emission peak at E_g in the device fabricated by annealing for 30 min (Fig. 6(d)). On the other hand, a peak (downward pointing arrow in the figure) appeared in the region corresponding to the photon energy $h\nu$ ($= 0.95$ eV, wavelength 1.3 µm) of the light radiated during annealing, which indicates that an optical near field was generated by this irradiation light, which restricted the annealing rate. In addition, the peak in the low-energy region (0.83 eV) was higher than in Fig. 6(c). Specifically, the

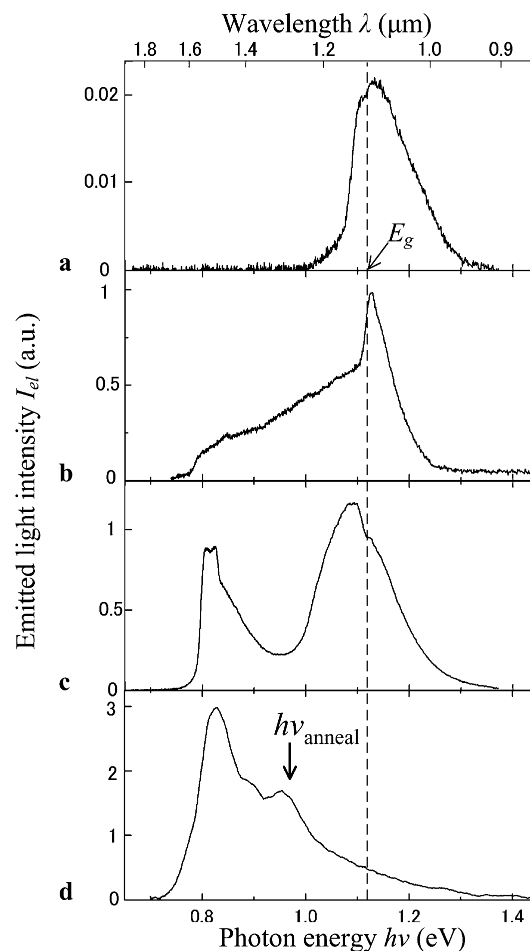

Fig. 6 Emission spectra. (**a**) Emission spectrum of commercially available Si photodiode (Hamamatsu Photonics K.K., S3590). (**b**)–(**d**) Emission spectra of fabricated devices. Annealing times were 1 minute (**b**), 7 minutes (**c**), and 30 minute (**d**)

emission intensity at this peak position was 14 times higher and 3.4 times higher compared with Figs. 6(b) and (c), respectively. The emission spectrum was distributed over energies 0.73–1.24 eV (wavelengths 1.00–1.70 µm), which covers the optical fiber communication band. The width of this range is 0.51 eV, which is at least four times larger than the spectral width of 0.12 eV of a commercially available InGaAs LED (Hamamatsu Photonics K.K., L10823) with an emission wavelength of about 1.6 µm.

Third, Figs. 7(a) and (b) show the relationship between the output optical power P_o and the electrical driving power P_e of the device fabricated by annealing for 30 min. The gradient of the straight broken line corresponds to the differential external power conversion efficiency. Figure 7(a) shows the results of measuring the power of the emitted light in the energy region higher than the photon energy $h\nu = 0.73$ eV (wavelength 1.70 µm). When 11 W of electrical power was applied, the external power conversion efficiency was 1.3%, and the differential external power con-

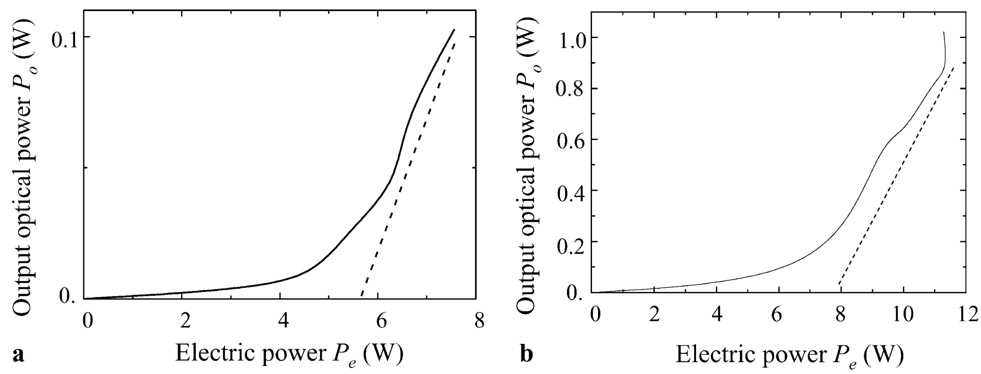

Fig. 7 Relationship between applied electrical power P_e and emitted optical power P_o. (**a**) Total power of emitted light in photon energy region 0.73 eV and above. Gradient of *broken line* corresponds to differential external power conversion efficiency of 5.0%. (**b**) Total power of emitted light in photon energy region 0.11–4.96 eV. Gradient of *broken line* corresponds to differential external power conversion efficiency of 40%

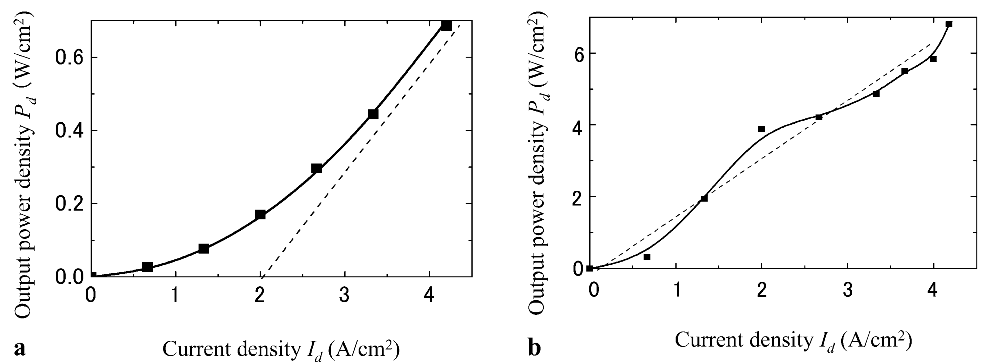

Fig. 8 Relationship between injected current density I_d and emitted optical power density P_d. (**a**) *Squares* are measured values of total power density of emitted light in photon energy region 0.73 eV and above. *Solid curve* represents quadratic curve $P_d = 0.04I_d^2$. Gradient of *broken line* corresponds to differential external quantum efficiency of 40%. (**b**) *Squares* are measured values of total power density of emitted light in photon energy region 0.11–4.96 eV. Gradient of *broken line* corresponds to external quantum efficiency of 50%

version efficiency was 5.0%. Because of the current limit of the power supply, it was not possible to input a power higher than this; however, even if a higher power could be applied, the device can stably operate without being damaged. Figure 7(b) shows the relationship between P_o and P_e in the photon energy region $h\nu = 0.11$–4.96 eV (wavelength 0.25–11.0 μm). An external power conversion efficiency of 10% and an external differential power conversion efficiency of 25% were achieved. However, this also included infrared radiation due to heating of the device, which will be necessary to examine in more detail.

To obtain the quantum efficiency, Fig. 8 shows the relationship between the emitted optical power density (P_d) and the current density (I_d) of the device fabricated by annealing for 30 min. Figure 8(a) shows the value of P_d in the energy region higher than the photon energy $h\nu = 0.73$ eV (wavelength 1.70 μm). The measured values, indicated by the squares, were fitted by the quadratic curve $P_d = 0.04I_d^2$ shown by the solid curve. In other words, in contrast to conventional devices in which P_d is proportional to I_d, in this device P_d is proportional to I_d^2. This is because the two-step spontaneous emission process described in Sect. 2 is dominant; in other words, a single electron is converted to two photons. When I_d was 4.0 A/cm^2, the external quantum efficiency was 15%. When I_d was 3.0–4.0 A/cm^2, the differential external quantum efficiency was 40%. Figure 8(b) shows the relationship between P_d and I_d in the photon energy region $h\nu = 0.11$–4.96 eV (wavelength 0.25–11.0 μm). The external quantum efficiency reached as high as 150%. The reason why this value is greater than 100% is because a single electron is converted to two photons by the two-step spontaneous emission process, as described above. However, the measured values of I_d in Fig. 8(b) also include the effects of infrared radiation due to heating of the device, which it will be necessary to examine in more detail.

If the thickness of the high-resistivity Si crystal wafer used in this method could be reduced, the electrical efficiency could be increased even more. Also, because the current density can be increased, if a method of increasing the efficiency of extracting light outside the device could be de-

vised, it should be possible to realize an LED with even higher efficiency and a wider band. This approach can also be applied to laser oscillators, and we plan to publish more details of this in a separate article.

5 Conclusion

Using stimulated emission triggered by an optical near field generated at the inhomogeneous domain boundary of B doped in Si, we controlled annealing with current injection and fabricated a high-efficiency, broadband LED. This device emitted light by means of a two-step phonon-assisted process due to the optical near field generated at the inhomogeneous domain boundary of B. Even though we used bulk crystal Si with a simple homojunction structure, the obtained emission band of the device extended over energies 0.73–1.24 eV, and with 11 W of input electrical power, the total optical power was as high as 1.1 W. The external power conversion efficiency was 1.3%, the differential external power conversion efficiency was 5.0%, the external quantum efficiency was 15%, and the differential external quantum efficiency was 40%.

Open Access This article is distributed under the terms of the Creative Commons Attribution Noncommercial License which permits any noncommercial use, distribution, and reproduction in any medium, provided the original author(s) and source are credited.

References

1. T.P. Lee, C.A. Burus, A.G. Dentai, IEEE J. Quantum Electron. **17**, 232 (1981)
2. R.A. Milano, P.D. Dapkus, G.E. Stillman, IEEE Trans. Electron Devices **29**, 266 (1982)
3. U.S. Department of Health and Human Services, Public Health Service, National Institute of Health, National toxicology program: NTP technical report on the toxicology and carcinogenesis studies of indium phosphide (CAS No. 22398-80-7) in F344/N rats and B6C3F1 mice (inhalation studies), NTP TR 499 (2001)
4. K.D. Hirschman, L. Tysbekov, S.P. Duttagupta, P.M. Fauchet, Nature **384**, 338 (1996)
5. Z.H. Lu, D.J. Lockwood, J.-M. Baribeau, Nature **378**, 258 (1995)
6. L. Dal Negro, R. Li, J. Warga, S.N. Basu, Appl. Phys. Lett. **92**, 181105 (2008)
7. T. Komoda, Nucl. Instrum. Methods Phys. Res., Sect. B, Beam Interact. Mater. Atoms **96**, 387 (1995)
8. S. Yerci, R. Li, L. Dal Negro, Appl. Phys. Lett. **97**, 081109 (2010)
9. S.K. Ray, S. Das, R.K. Singha, S. Manna, A. Dhar, Nanoscale Res. Lett. **6**, 224 (2011)
10. M.A. Green, J. Zhao, A. Wang, P.J. Reece, M. Gal, Nature **412**, 805 (2001)
11. T. Kawazoe, K. Kobayashi, S. Takubo, M. Ohtsu, J. Chem. Phys. **122**, 024715 (2005)
12. S. Yukutake, T. Kawazoe, T. Yatsui, W. Nomura, K. Kitamura, M. Ohtsu, Appl. Phys. B, Lasers Opt. **99**, 415 (2010)
13. T. Kawazoe, M. Ohtsu, Y. Inao, R. Kuroda, J. Nanophotonics **1**, 011595 (2007)
14. T. Yatsui, K. Hirata, W. Nomura, Y. Tabata, M. Ohtsu, Appl. Phys. B **93**, 55 (2008)
15. T. Kawazoe, H. Fujiwara, K. Kobayashi, M. Ohtsu, IEEE J. Sel. Top. Quantum Electron. **15**, 1380 (2009)
16. Y. Tanaka, K. Kobayashi, Physica E **40**, 297 (2007)
17. M.G.A. Bernard, G. Duraffourg, Phys. Status Solidi **1**, 699 (1961)
18. R.J. Van Overstraeten, R.P. Mertens, Solid-State Electron. **30**, 1077 (1987)
19. J.A. Van den Berg, D.G. Armour, S. Zhang, S. Whelan, H. Ohno, T.-S. Wang, A.G. Cullis, E.H.J. Collart, R.D. Goldberg, P. Bailey, T.C.Q. Noakes, J. Vac. Sci. Technol. B **20**, 974 (2002)
20. A. Einstein, P. Ehrenfest, Z. Phys. **19**, 301 (1923)
21. E. Shl, *Nonequilibrium Phase Transitions in Semiconductors* (Springer, Berlin, 1987), pp. 5–6